ORIGINAL RESEARCH ARTICLE



Toward Highly Dense Yb-Silicate Microstructures Deposited by Air Plasma Spray for Environmental Barrier Coating Applications I: Influence of Local Deposition Rate

Emine Bakan¹ • Edward J. Gildersleeve V¹ • Robert Vaßen¹

Submitted: 29 September 2024/in revised form: 31 December 2024/Accepted: 17 January 2025/Published online: 2 April 2025 © The Author(s) 2025

Abstract Environmental barrier coatings (EBCs) are used to shield high-temperature Si-based ceramic matrix composite gas turbine components from the harsh, water vaporrich operating environment. The success of this application is directly correlated to the intrinsic gas tightness or hermeticity of the EBC volatilization barrier, which are typically rare-earth disilicates. For the air plasma-sprayed (APS) EBCs, the hermeticity is directly related to the processing parameters during deposition. In this work, the effect of surface speed and feeding rate on the microstructural evolution of plasma-sprayed Yb₂Si₂O₇ coatings was studied. A qualitative assessment by means of microstructure analysis of hermeticity after crystallization heat treatment and the influence of the aforementioned processing parameters is discussed. It was found that utilizing lower feeding rates can minimize certain types of disadvantageous cracking in the as-deposited Yb₂Si₂O₇ coatings. Moreover, at these low feeding rates ($\sim 1-5.4$ g/ min) regardless of the selected surface speed (250-1250 mm/s), highly dense Yb₂Si₂O₇ microstructures could be obtained in the as-sprayed state. Contrastingly at higher feeding rates (~ 46.2 g/min), deleterious Yb₂SiO₅ band formation was observed at the top of each spray pass, which correlated to worsened cracking in the microstructures, particularly at low surface speed (250 mm/s). The monosilicate band formation was linked to the fine particle fraction of the feedstock (i.e., particles $< 15 \mu m$), and by sieving out this fraction the band formation could be eliminated when spraying at the higher feeding rate.

Keywords APS \cdot EBCs \cdot hermeticity \cdot local deposition rate \cdot microstructural evolution \cdot Yb₂Si₂O₇

Introduction

SiC-based ceramic matrix composites (CMCs) are considered more advanced than Ni-based superalloys for gas turbine applications due to their superior high-temperature performance, reduced weight, and enhanced thermal stability (Ref 1-4). However, all SiC-based materials for use in high-temperature combustion environments also need protective coatings because of the volatilization of thermally-grown silica upon water vapor impingement (Ref 5, 6). So-called Environmental Barrier Coatings (EBCs) are used for this purpose. State of the art EBCs are typically two-layer structures that consist of an intermediary bond coat (Si) and volatilization barrier top coat (e.g., (Y and/or Yb)₂Si₂O₇) (Ref 7-9) (Ref 10-14). For optimal performance, the volatilization barrier should be gas-tight/ hermetic in order to shield the Si-based materials (either the SiO₂-forming Si bond coat or the SiC substrate) from impinging water vapor. However, established manufacturing methods for fabricating Yb-silicate layers, in particular thermal spraying, have faced challenges in building hermetic coatings. These challenges stem from both the formation of secondary phases with higher thermal expansion coefficients (CTE) and the as-fabricated amorphous structure of the coating (Ref 12, 13).

In the APS process, the formation of secondary phases is attributed to the inflight vaporization or volatilization of SiO species from molten Yb₂Si₂O₇ particles, resulting in the deposition of SiO₂-depleted Yb-silicate phases; primarily these inflight-volatilized-particles manifest in the coatings as a mixture of Yb₂O₃ and Yb₂SiO₅ (Ref 15). The



Emine Bakan e.bakan@fz-juelich.de

Forschungszentrum Jülich GmbH, Institute of Energy Materials and Devices (IMD-2), 52425 Jülich, Germany

CTE of Yb₂SiO₅ is 7.2 ppm/K while the Si, SiC and Yb₂Si₂O₇ have CTEs in the range of 4-5 ppm/K (Ref 16). Consequently, the amount of Yb₂SiO₅ in the Yb₂Si₂O₇ coating will dictate the CTE mismatch stresses in the system. According to high-temperature x-ray diffraction and dilatometric measurements, both of which are used to determine the crystallization temperature of materials/coatings, Yb₂Si₂O₇/Yb₂SiO₅ coatings start to crystallize at about 1000 °C (depending on the heating rate chosen) (Ref 17, 18). In traditional APS processing, maintaining steady-state component temperatures at this magnitude is not possible. As such, rapidly quenched Yb₂Si₂O₇/Yb₂SiO₅ particles impinging the Si-coated SiC substrate will remain amorphous upon deposition. The as-deposited crystallinity content has been shown to be controllable by increasing the deposition temperatures above 1000 °C by plasma spraying onto samples contained in a furnace (Ref 19) or, alternatively, plasma heating in very low pressure plasma spray processes (Ref 12). However, the scalability and feasibility of such processing remains questionable. Therefore, in most cases, the post-deposition crystallization heat treatment will be applied and lead to microstructural changes in the Yb₂Si₂O₇ coating. For example, spherical pore formation in the place of the as-deposited microcracks; based on an in-depth image analysis study, the evolution of the microstructure after crystallization results in an increase in the total porosity of the coating (Ref 20).

In traditionally plasma-sprayed ceramic materials, the porosity (prior to any subsequent heat treatment) that is observed stems from a combination of factors. The rapid microsecond quenching from the molten/liquid state while constrained to a rigid substrate results in the development of substantial stresses (Ref 21, 22). These quenching stresses contribute to the formation and evolution of through-thickness channel cracking on the individual droplet (or splat) level, which then manifests in coatings as microcracks (Ref 23-25). In addition, processing gases can be captured and entrapped within the molten droplets in flight as well as in the coating itself as successive droplets impact the substrate—which forms in the coating as spherical or globular porosity (Ref 26-28). Lastly, horizontal, or lateral (in 2D) cracks and/or delaminations that run parallel to the coating-substrate interface can form due to either poor splat-to-splat bonding or in response to stresses surrounding the aforementioned existing microcracks (Ref 23-25). In the case of microstructural evolution during heat treatment and crystallization of APS Yb₂Si₂O₇ EBCs, it was found that each of these unique pore features in a plasma-sprayed coating evolve differently from each other (Ref 20). An example of this can be seen in Fig. 1 which shows the microstructure of an air plasma-sprayed Yb₂Si₂O₇ coating (see plasma spray condition #1 in Table 1 in the experimental section) in the as-sprayed/ amorphous state (Fig. 1a) and after crystallization heat treatments (Fig. 1b-c). Horizontal arrows (blue) mark the vertical microcracks (intralamellar cracks) in the microstructures while tilted arrows (orange) indicate the horizontal cracks (interlamellar cracks). It can be seen that even after a single-step high-temperature heat treatment (Fig. 1b, 20 h at 1300 °C, hereinafter will be referred to as the 'standard heat treatment'), the vertical microcracks nearly disappear, as they transform into spherical pores due to viscous flow (Ref 20). After the two-step heat treatment (Fig. 1c, 40 h 975 °C + 10 h at 1300 °C), which was designed to suppress the viscous flow (Ref 20), vertical cracks are still visible in the microstructure. However, regardless of which heat treatment is chosen, horizontal

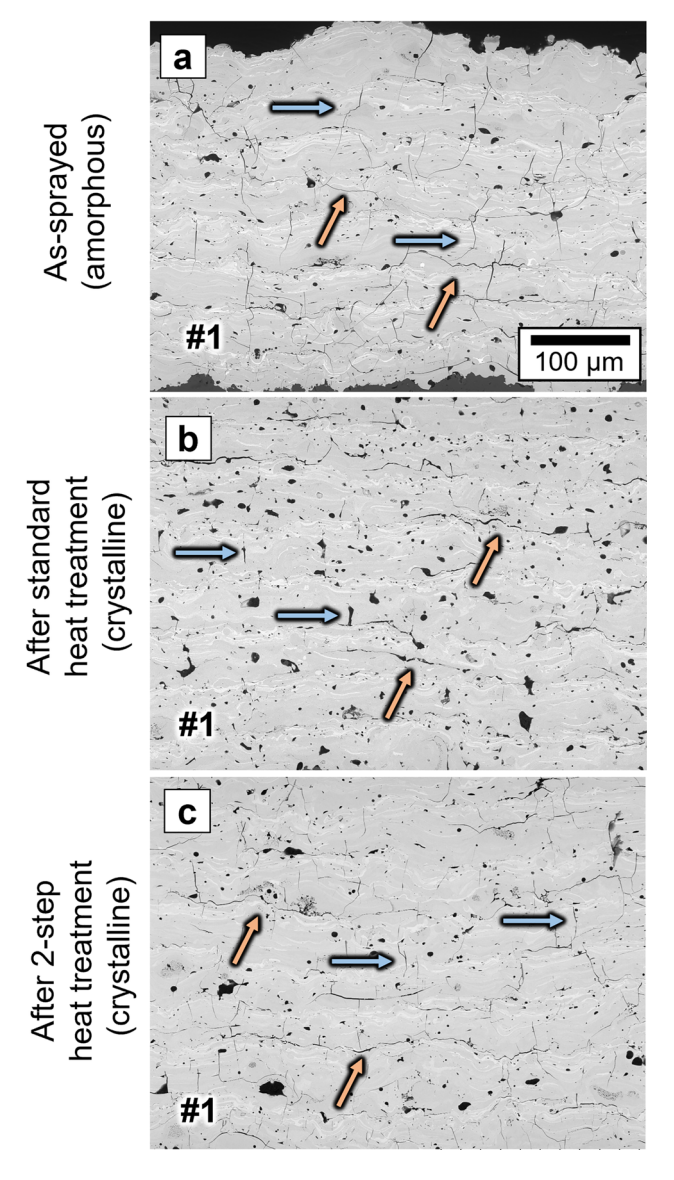


Fig. 1 Backscatter SEM microstructure of air plasma-sprayed $Yb_2Si_2O_7$ coating in the as-sprayed state (a), after 20 h at 1300 °C (b), after 40 h 975 °C + 10 h at 1300 °C (c)



cracks always remain in the microstructure (Fig. 1b,c). Moreover, the horizontal cracks appear to open more aggressively during the standard heat treatment (clearly a debit to final hermeticity), again indicating microstructural dependency on the viscous flow of material (Fig. 1b). Answering the question of why horizontal cracks do not transform into spherical pores as the vertical microcracks do is beyond the scope of this study. However, it is clear that, if one can reduce the number of horizontal cracks in the as-sprayed microstructure, the overall hermeticity of the EBC can be improved, even after a single-step heat treatment.

Therefore, in this study, reducing the as-deposited porosity, more specifically minimizing the number of horizontal cracks was targeted. From the published literature, there are very limited works that approach the horizontal cracks in plasma-sprayed ceramic coatings specifically. It is only known that utilizing a higher torch power (e.g., by increasing the spray current), results in lower porosity levels in the as-sprayed microstructure due to higher particle temperatures subsequently more wellmolten particles in the spray stream (Ref 20, 29-33). It was also shown that by increasing the H₂ content of plasma gas at a constant spray current, which also increases the torch power, the same effect can be observed (Ref 13). However, to the best of the authors' knowledge, there is no systematic study published investigating the relation between the unique crack geometries (e.g., horizontal and vertical

Table 1 Variation of surface speed and feeding rate at different experiments. Note that the number of passes were adjusted in each experiment to achieve a similar coating thickness (300-400 μ m)

Experiment	Surface speed, mm/ s	Feeding rate, g/min	Number of passes	Thickness per pass, μm
#1 (Baseline)	500	23.1	8	50
#2	250	5.4	16	23
#3	1250	46.2	9	36
#4	250	46.2	2	200
#5	1250	5.4	55	6
#6	250	1	85	4

Table 2 Yb₂Si₂O₇ feedstock air plasma spray conditions

Spray parameters				
Plasma gas composition	49 slpm Ar, 1slpm H ₂			
Spray current	325 A			
Spray distance	90 mm			
Nozzle diameter	9 mm			
Raster speed	250-1250 mm, s varied			
Feeding rate	1-46.2 g, min <i>varied</i>			

microcracks) and individual process parameters. Thus, the effect of surface speed and feeding rate, which determine the local deposition rate, on the formation of crack patterns was investigated in this study. For simplicity, the concept of 'local deposition rate' is an amalgamation of the particle feeding rate and torch-to-component surface speed which captures the local 'amount of material' that is deposited in a single point in space/time. The experiments were designed around understanding how the horizontal crack concentration specific to APS Yb2Si2O7 can be controlled based on the local deposition rate. From these results, a strategy toward designing processing conditions for APS EBCs while simultaneously bearing the final heat-treated microstructural evolution mechanisms in mind is presented.

Materials and Method

The Yb-silicate coatings were manufactured by using a commercial $Yb_2Si_2O_7$ feedstock $(d_{10}/d_{50}/d_{90} = 14/28/$ 57 μm, Höganäs, Sweden) in a MultiCoat system (Oerlikon Metco, Wohlen, Switzerland) with a three-cathode TriplexPro 210 spray torch mounted on a six-axis robot (IRB 2400, ABB, Switzerland). The Yb₂Si₂O₇ feedstock did not contain any secondary Yb2SiO5 phases; the XRD diffractogram of the powder can be found in the supplementary file. The plasma spray conditions are summarized in Tables 1 and 2. Because the local deposition rate was modulated throughout this study, it was important to constrain the final as-deposited coating thickness as rigorously as possible, so as to avoid undesired microstructural artifacts due to increased/decreased coating thicknesses (Ref 23). The experiments were broken down systematically in an effort to isolate the individual contributing components of the local deposition rate (feed rate and surface speed) and resolve their individual contribution to the as-deposited microstructure. A typical ladder-style meander pattern was used to deposit the coatings in this study. The meander width was 200 mm for all experiments with a step size of 2 mm. In total 16 strokes were used to cover the entire surface of 25 \times 25 \times 3 mm Si bond-coated sintered α -SiC substrates (Saint Gobain Ceramics, Niagara Falls, NY). Si



bond coat spraying conditions and feedstock information can be found elsewhere (Ref 34).

Specimen temperatures were measured during deposition from the front and backside of the specimen using a NiCr thermocouple (Omega Engineering, Deckenpfronn, Germany, data acquisition 1 Hz) attached to the back of the samples as well as an infrared camera (Xi 400, Optris, Berlin, Germany, data acquisition 30 Hz) from the specimen surface, assuming the emissivity as 1 leading the infrared camera to underestimate the temperature. An area of approximately $10 \times 10 \text{ mm}^2$ at the center position of the substrate was used for the IR camera measurements and a temperature range of 150-900 °C was chosen from the software. Particle diagnostics during spraying were performed using the commercially available DPV Millenium Edition (Tecnar Inc., QA, Canada) (Ref 35). It is critical to note that for all experiments in this study, particle injection optimization was carried out to ensure uniform, consistent, and reproducible particle-plume interactions from run-torun (Ref 36). Measurements of the particle state were taken in two modes: at the center of maximum counted particles within the plume and as a 30×2 mm grid with a step size of 1 mm and measurement time of 1000 ms or 1000 particles per data point, whichever comes first. Metallographic cross sections of the coatings were prepared for microstructural investigations via scanning electron microscopy (SEM, TM-3000, Hitachi, Tokyo, Japan).

Results and Discussion

Effect of Surface Speed and Feeding Rate on Coating Microstructure

In order to explore the effect of surface speed and feeding rate on coating microstructure, initially two spray experiments (Table 1, #2-3) were conducted for comparison with the baseline spray condition #1 (Fig. 1). Figure 2 shows the microstructure of these coatings in the as-sprayed state (a, b) as well as after crystallization heat treatments (a1, a2, b1, b2). It can be seen from the micrographs that lowering the surface speed and feeding rate at the same time (#2) was productive in minimizing horizontal cracks in the microstructure (Fig. 2a, a1, a2). Whereas a higher surface speed and feeding rate clearly generated the opposite effect (Fig. 3b, b1, b2). The reasons for these differences from a process-microstructure perspective are discussed below.

Improved interlamellar bonding in thermally sprayed ceramic coating microstructures has been linked in the past to higher deposition temperatures (Ref 37, 38). Given the choice of reducing the surface speed for experiment #2, it was plausible to consider the microstructure result in Fig. 2 as a consequence of increased deposition temperatures.

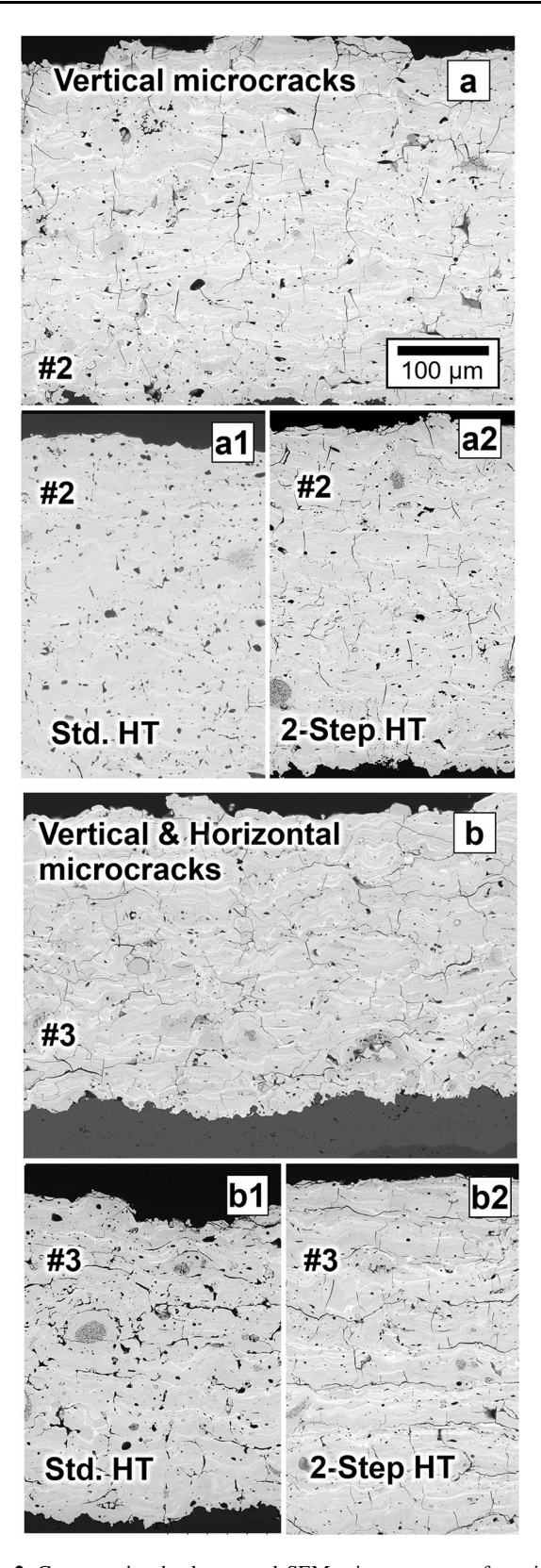


Fig. 2 Cross-section backscattered SEM microstructure of coatings produced using spray condition #2 (a, a1, a2), and #3 (b, b1, b2). Images (a), (b) show the as-sprayed microstructure, (a1), (b1), and (a2), (b2) are the microstructures after standard and two-step heat treatments, respectively



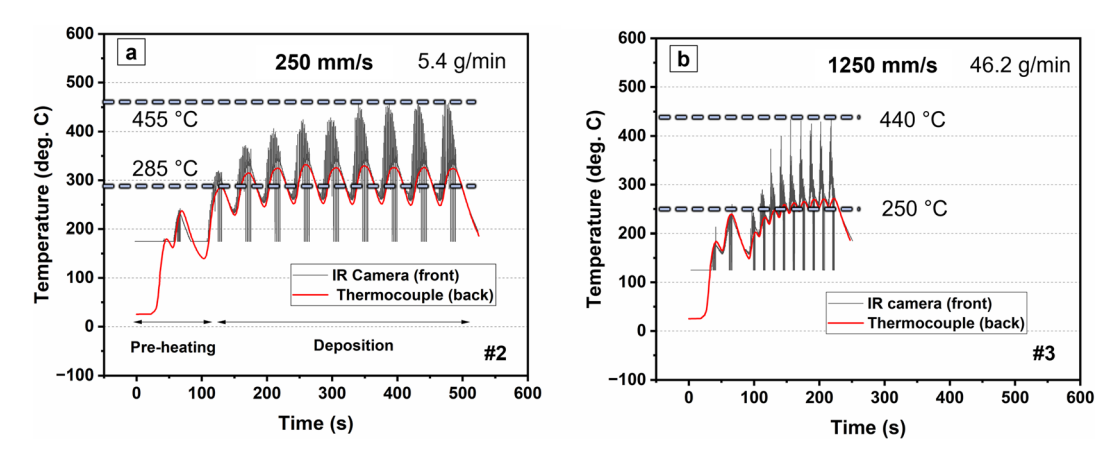


Fig. 3 Temperature measurements of samples during plasma spraying under conditions #2 (a) and #3 (b). Note that pre-heating conditions (500 mm/s, 2 passes) were the same in both experiments (in all experiments)

Therefore, measured deposition temperatures at the lowest (experiment #2) and highest surface speed (experiment #3) spray conditions were compared, as shown in Fig. 3. The thermocouple readings revealed much less scattering due to lower data acquisition frequency in comparison with the thermal camera, however average temperatures measured with both methods appeared consistent. As indicated by the line drawn through the datasets, the average deposition temperatures were measured as \sim 285 and \sim 250 °C at experimental conditions #2 and #3, respectively. Of course, the specimen surface undergoes extreme thermal excursions as the spray plume impacts and traverses along. While the IR camera was sampling at its maximum allowable frequency, it is likely that ultra-localized temperatures were higher than what is resolvable by this technique. Nevertheless, the maximum deposition temperatures acquired from IR camera were compared for equivalent sampling and spatial conditions. As seen in Fig. 3, the maximum temperature data were also quite similar (455 vs. 440 °C) in both spray conditions. Based on these, with the available temperature measurement techniques, it could not be confirmed that lower surface speeds result in significantly higher deposition temperatures for this APS EBC process. One possible explanation could be due to the concurrent reduction of the feeding rate used in this experiment #2, which would inevitably lower the heat load onto the specimen. From these conclusions, it was necessary to explore the opposite extremes: low surface speeds with higher feeding rates and vice versa.

Figure 4 shows the cross-section microstructure of the coatings sprayed with conditions #4-5 (Table 1) to make a direct comparison with #2-3, respectively. When a low surface speed combined with a high feeding rate is used, a Yb₂SiO₅-rich band (evident with the brighter backscatter contrast) was observed at the top region of each deposition pass, as indicated in Fig. 4a-a1. Through-thickness

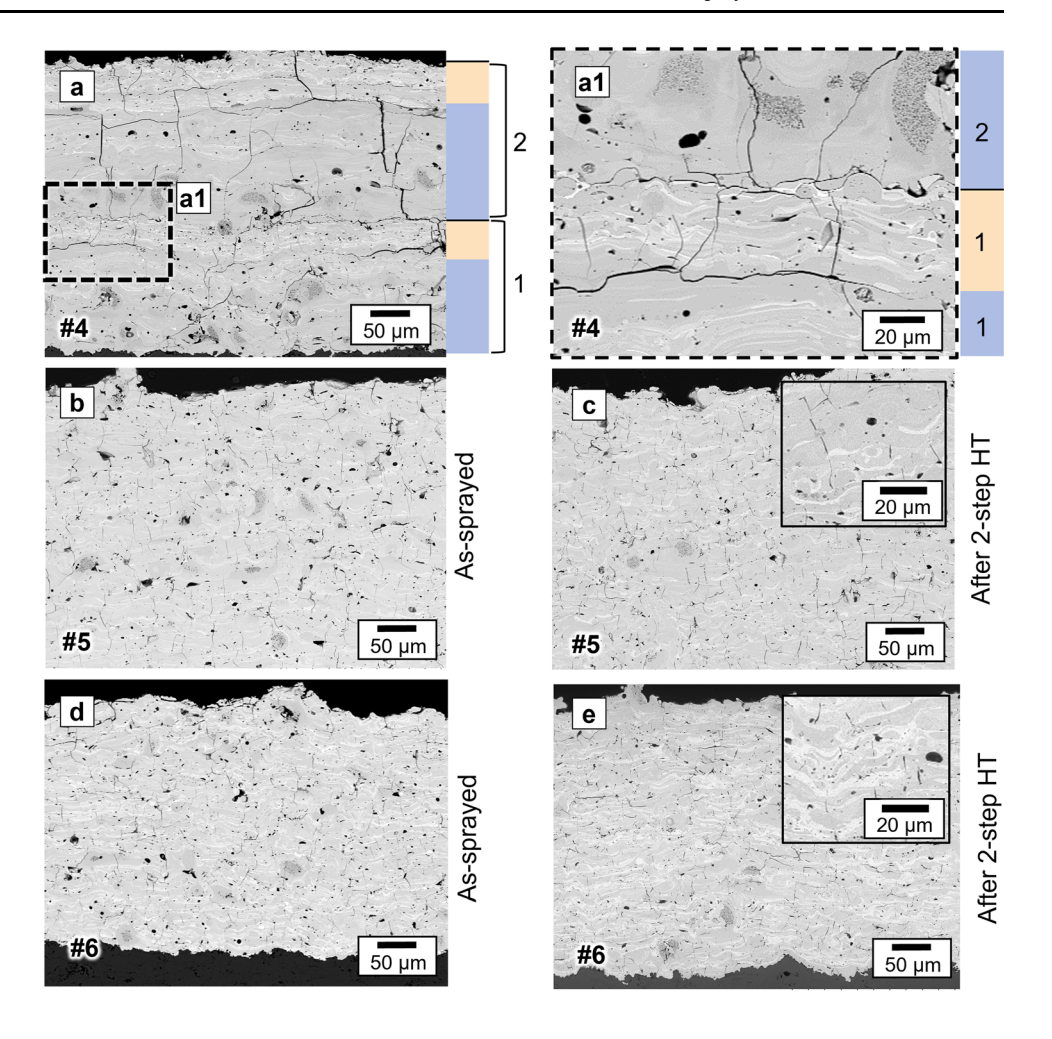
mudcracks formed in this layer which seemed to bifurcate at the Yb_2SiO_5 -rich/ $Yb_2Si_2O_7$ boundary (marked with yellow and blue boxes, respectively). Presumably, these vertical mudcracks were initiated due to the higher CTE of Yb_2SiO_5 , which led to the manifestation of in-plane tensile stresses in the Yb_2SiO_5 -rich band during cooling as the torch departed. The mud cracks bifurcated at the Yb_2SiO_5 -rich/ $Yb_2Si_2O_7$ interface suggesting the propagating crack front experienced compressive stresses due to the CTE mismatch.

The vertical mud cracks can also be found at the top region of the first pass (Fig. 4a1), and these cracks probably acted as an initiation point for vertical cracks to propagate into the second pass, which would result in the presence of vertical cracks through the thickness of the $Yb_2Si_2O_7$ -rich (Fig. 4a1, blue box #2) region. This would explain why such vertical cracks were not observed in the $Yb_2Si_2O_7$ -rich region of the first pass. On the one hand, the Yb_2SiO_5 band appeared to exacerbate the cracking in the microstructure. However, it cannot be discounted that a high single-pass deposition thickness (150-200 μ m) might have contributed to the observed cracking in the microstructure (stored elastic strain energy is proportional to the thickness (Ref 39)), as well. The reason of Yb_2SiO_5 band formation will be further discussed below.

In contrast to the highly cracked microstructure obtained using spray condition #4, condition #5 yielded a highly dense microstructure (Fig. 4b-c). Horizontal cracks were significantly minimized, and due to low pass thickness (Table 1), intralamellar cracks were also smaller in comparison with #2 (Fig. 2a) where the feeding rate was consistent but the surface speed was lower (250 mm/s as opposed to 1250 mm/s). This experimental result also confirmed that for the APS EBC deposition process, the deposition temperature, which was even slightly lower than #3 (average ~ 220 °C), does not seem to play a decisive



Fig. 4 Cross-section backscattered SEM images of the coatings sprayed with conditions #4 (a, a1), #5 (b, c) and #6 (d, e). Yellow and blue boxes in (a) and (a1) are marking Yb₂SiO₅-rich and Yb₂Si₂O₇-rich sections in the coating sprayed using two passes, respectively. (a), (a1), (b) and (d) are as-sprayed, (c) and (e) are 2-step heat-treated microstructures



role in the formation of horizontal cracking. From the microstructural comparisons of #2-3-4-5, it was concluded that the low feeding rate was unilaterally beneficial to minimize the horizontal cracking in the microstructure regardless of whether low or high surface speeds were used. One hypothesis is that, intralamellar (vertical) microcracks may be promoting the initiation of horizontal cracks if there is sufficient energy stored. By reducing the pass thickness through using a lower feeding rate, the available elastic strain energy that could drive 3-dimensional microcrack propagation (intralamellar crack extension and interlamellar crack initiation) was also reduced. In order to validate this hypothesis, and assess if the intralamellar crack length could be further reduced, a final experiment (#6) was performed using an ultra-low feeding rate. The microstructure of this coating be seen in Fig. 4 (de). Supporting the previous findings, regardless of the low raster speed, the horizontal cracks were minimized and the vertical crack length could be reduced down to the 3-4 μm range (Fig. 4e, inset).

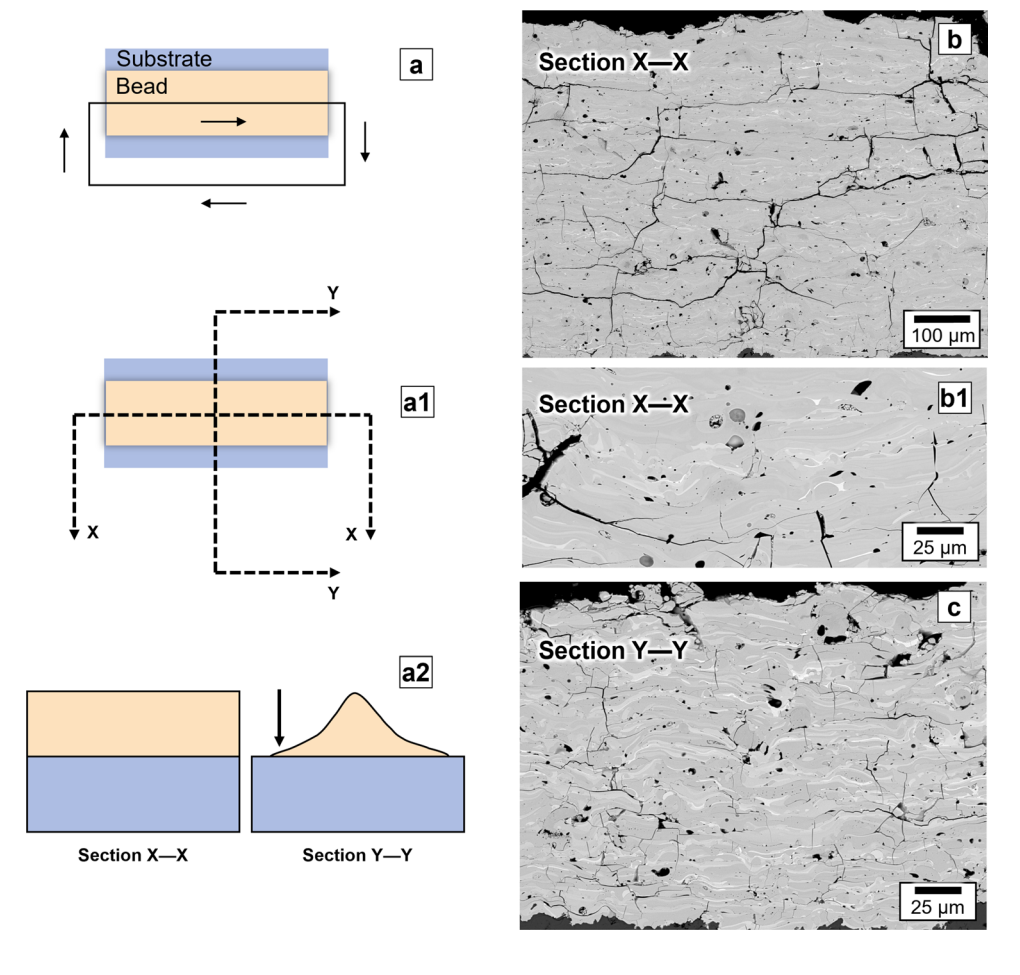
Understanding the Formation of the Yb₂SiO₅ Band at High Feeding Rates and Removing it Completely

In order to investigate the Yb_2SiO_5 band formation, a specialized robotic toolpath used in a prior work to understand the evolution of the coating microstructure based on a spatial understanding of the spray plume was used (Ref 40). This 'bead experiment' was performed as demonstrated in Fig. 5a, where robot makes a loop rather than following a ladder pattern. The spraying conditions were identical to #4 (250 mm/s, 46.2 g/min), where the Yb_2SiO_5 band formation was observed, notwithstanding the modified robot toolpath.

Note that the Yb_2SiO_5 banding is hypothesized to have also formed at spray condition #3, where also high feeding rate was used (Fig. 2b, b1, b2). However, as the pass thickness was lower due to higher surface speed (1250 mm/s) at #3, the thickness of the individual Yb_2SiO_5 bands should be smaller, and therefore it was more difficult to discern it. For that reason, the bead experiment was performed at the lower surface speed. Figure. 5 shows the cross-section images taken from the centerline of the bead



Fig. 5 Schematic of the bead experiment (a), made cross sections (a1) and thickness distribution of the bead in different cross sections (a2). Arrows in (a) show the trajectory of the robot during the experiment and the position of the SEM image taken in (a2). Backscattered SEM images were taken from the centerline (section X-X) of the bead (b, b1) and as well as from section Y-Y (c)



(section X-X) (b, b1) at different magnifications as well as from the fringe of the bead (section Y-Y) (c). Due to Gaussian distribution of particles, the thickness at the centerline of the bead (Fig. 5b, b1) was significantly thicker than the fringes (Fig. 5c). Additionally, it was evident from the image contrast that the chemical composition of the EBC layer was different at the centerline when compared to the fringes, i.e., the centerline contained significantly less amount of Yb_2SiO_5 (the phase with lighter backscatter contrast).

These new bead results suggested that there should be considerable deviations in the spatial distribution of particle states in the plume. Therefore, particle diagnostic measurements as outlined in the Methods section were performed using the same deposition conditions (#4, note that the robot is stationary during these measurements) to map the spatial distribution of particle flow rate, temperature and diameters in the plume as shown in Fig. 6. Particle flow rate showed a symmetrical distribution, with the highest flow rate located at the center, which gradually reduced toward upper and lower fringes (Fig. 6a). Particle diameters on the other hand were rather asymmetrical, particles with a diameter smaller than 15 μ m were found in

the upper half of the plume cross section (toward the injection point) while larger particles were detected in the lower half (toward the ground, Fig. 6c). Considering radial injection conditions used in this study this result is expected. Finer particles have a lower mass and therefore experience less momentum when entering the plasma plume compared to larger particles. As a result, finer particles are more likely to be carried along with the flow of the plasma plume (Ref 41). Correspondingly, particle temperatures were higher at the upper half and vice versa (Fig. 6b). The presence of simultaneously finer and hotter particles would imply particles existing with a more pronounced evaporation of SiO species from Yb₂Si₂O₇, it could explain the higher Yb₂SiO₅ content at the plume fringes as observed in the bead experiment (Fig. 5c).

In order to test this hypothesis, a second Yb₂Si₂O₇ feedstock (Oerlikon Metco Inc. Westbury, NY, USA) was sieved to remove the fine particle fraction and used for another experiment. Because there was an insufficient amount of powder left at this point from the original experiments for further testing. After sieving, the second feedstock had a size distribution of $d_{10}/d_{50}/d_{90} = 26/46/71$ µm. Here again, injection optimization experiments



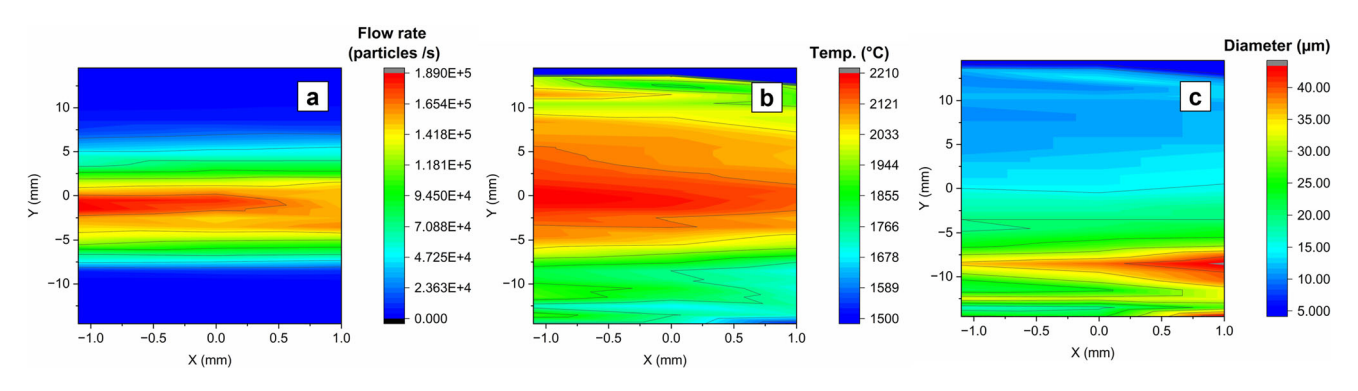


Fig. 6 Particle flow rate (a), particle temperature (b) and particle diameter (c) maps in plasma plume cross section

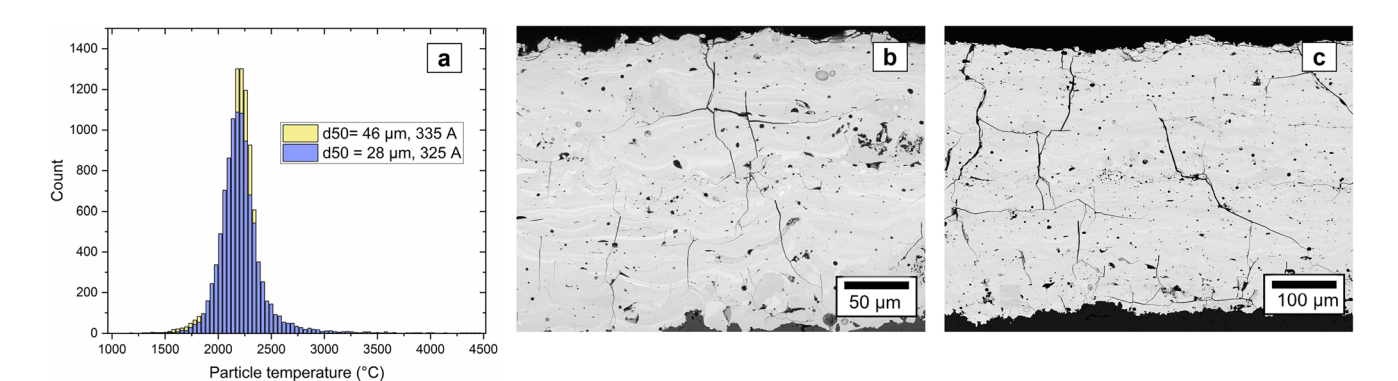


Fig. 7 Particle temperature measurements of the two $Yb_2Si_2O_7$ feedstock ($d_{50} = 28 \mu m$ is the first feedstock, $d_{50} = 46 \mu m$ is the sieved feedstock) at different spray currents (a), cross-section

23.1 g/min (b) and 46.2 g/min (c) feeding rate coatings had large through-thickness and horizontal cracks, suggesting that not only the Yb_2SiO_5 band but also high

microstructure of the coatings sprayed at 335 A with the sieved

powder (the remaining spray parameters are identical to #4) using

were performed to determine the necessary carrier gas flow rates for all new feedstocks examined. Using this new sieved powder, firstly, particle injection optimization and temperature measurements were performed. It was determined that slightly different spray current levels were needed in order to match the particle temperature distribution with the original feedstock from earlier experiments while constraining auxiliary parameters like plasma gas flow rates. Matching particle temperature distributions (not average particle temperatures) was vital here to ensure there were as minimal differences to potential SiO volatilization inflight as possible. As shown in Fig. 7a, such a temperature-matched could be obtained at 335 A using the second feedstock, i.e., a larger particle size distribution required a slightly higher spray current to reach the same particle temperature range. After that, coatings were sprayed using the 250 mm/s surface speed and both 23.1 g/ min and 46.2 g/min feeding rates (similar to spray condition #4) but with the new 335 A spray current. The microstructure of the coatings as shown in Fig. 7b-c revealed no Yb₂SiO₅ band, regardless of the presence of Yb₂SiO₅ phase in the feedstock (XRD diffractogram (S2) can be seen in the supplementary file). Nevertheless, the

suggesting that not only the Yb₂SiO₅ band but also high pass thickness promotes cracking in the microstructure. This will be explored further in the second part of this study.

Conclusions

This study aimed to tailor spray processing conditions to eliminate as many of the horizontal cracks and/or delaminations in APS EBCs as possible in the as-deposited state. To that end, it became necessary to understand the driving force(s) and controllable input processing parameters that could effectively alter that horizontal crack concentration. The effects of surface speed and feeding rates (i.e., the local deposition rate) in the air plasma spray process on EBC coating microstructure were investigated. It was found that;

 Horizontal cracks can be significantly minimized by reducing the single-pass thickness, i.e., by utilizing lower-than-expected feeding rates; this benefit is seen regardless of slow/fast surface speeds.



- At high feeding rates, Yb₂SiO₅ bands were observed at the top surface of each spray pass. The thickness of the band was significantly larger at low surface speed conditions, and thereby cooldown-cracking due to CTE mismatch strains was substantially more obvious in the as-deposited microstructure.
- Particle diagnostics revealed that particles smaller than ~ 15 μm diameter, which were mainly found closer to the injection point, and their surface temperatures were higher than the larger particles at the lower portion of the plume. These finer, hotter particles were discerned to be the primary contributor to the Yb₂SiO₅ band formation by studying the plume profile bead cross section.
- By sieving out the fine particle fraction, the disadvantageous band formation could be eliminated, which simultaneously improved the cracking in the coating. However, high pass thickness for feedstock-optimized spraying runs was still found to be a contributor to the onset and propagation of large cooldown cracks (both horizontal and vertical) in the APS EBCs. Further experimental runs and spray condition design are thereby required to combine the optimal characteristics of these learnings in order to fabricate the most ideal as-deposited APS Yb₂Si₂O₇ microstructure that will subsequently densify toward a fully gas-tight hermetic coating.

Open Access This article is licensed under a Creative Commons Attribution 4.0 International License, which permits use, sharing, adaptation, distribution and reproduction in any medium or format, as long as you give appropriate credit to the original author(s) and the source, provide a link to the Creative Commons licence, and indicate if changes were made. The images or other third party material in this article are included in the article's Creative Commons licence, unless indicated otherwise in a credit line to the material. If material is not included in the article's Creative Commons licence and your intended use is not permitted by statutory regulation or exceeds the permitted use, you will need to obtain permission directly from the copyright holder. To view a copy of this licence, visit http://creativecommons.org/licenses/by/4.0/.

References

- 1. M. Belmonte, Advanced Ceramic Materials for High Temperature Applications, *Adv. Eng. Mater.*, 2006, **8**(8), p 693–703.
- R. Naslain and F. Christin, SiC-Matrix Composite Materials for Advanced Jet Engines, MRS Bull., 2011, 28(9), p 654–658.
- 3. M. Fellet and W. Rossner, Ceramic-Matrix Composites Take the Heat, *MRS Bull.*, 2015, **40**(11), p 916–918.
- N.P. Padture, Advanced Structural Ceramics in Aerospace Propulsion, *Nat. Mater.*, 2016, 15(8), p 804–809.
- N.S. Jacobson, E.J. Opila, and K.N. Lee, Oxidation and Corrosion of Ceramics and Ceramic Matrix Composites, *Curr. Opin. Solid State Mater. Sci.*, 2001, 5(4), p 301–309.

- E.J. Opila et al., SiC Recession Caused by SiO₂ Scale Volatility Under Combustion Conditions: II, Thermodynamics and Gaseous-Diffusion Model, *J. Am. Ceram. Soc.*, 1999, 82(7), p 1826–1834.
- K.N. Lee, R.A. Miller, and N.S. Jacobson, New Generation of Plasma-Sprayed Mullite Coatings on Silicon Carbide, *J. Am. Ceram. Soc.*, 1995, 78(3), p 705–710.
- 8. Eaton, H.E., et al. *EBC Protection of SiC/SiC Composites in the Gas Turbine Combustion Environment.* in *ASME Turbo Expo 2000: Power for Land, Sea, and Air.* 2000. American Society of Mechanical Engineers.
- Lee, K.N., Environmental Barrier Coatings For SiC/SiC, in Ceramic Matrix Composites: Materials, Modeling and Technology, N.P. Bansal and J. Lamon, Editors. 2015, The American Ceramic Society.
- B.T. Richards, M.R. Begley, and H.N.G. Wadley, Mechanisms of Ytterbium Monosilicate/Mullite/Silicon Coating Failure During Thermal Cycling in Water Vapor, *J. Am. Ceram. Soc.*, 2015, 98(12), p 4066–4075.
- B.T. Richards et al., Response of Ytterbium Disilicate–Silicon Environmental Barrier Coatings to Thermal Cycling in Water Vapor, Acta Mater., 2016, 106, p 1–14.
- E. Bakan et al., Yb₂Si₂O₇ Environmental Barrier Coatings Deposited by Various Thermal Spray Techniques: A Preliminary Comparative Study, *J. Therm. Spray Technol.*, 2017, 26(6), p. 1011–1024.
- E. Garcia, H. Lee, and S. Sampath, Phase and Microstructure Evolution in Plasma Sprayed Yb₂Si₂O₇ coatings, *J. Eur. Ceram.* Soc., 2019, 39(4), p 1477–1486.
- K.N. Lee, Yb₂Si₂O₇ Environmental Barrier Coatings with Reduced Bond Coat Oxidation Rates Via Chemical Modifications for Long Life, J. Am. Ceram. Soc., 2019, 102(3), p 1507–1521.
- B.T. Richards, H. Zhao, and H.N.G. Wadley, Structure, Composition, and Defect Control During Plasma Spray Deposition of Ytterbium Silicate Coatings, *J. Mater. Sci.*, 2015, 50(24), p 7939–7957.
- Z. Tian et al., Theoretical and Experimental Determination of the Major Thermo-Mechanical Properties of RE₂SiO₅ (RE = Tb, Dy, Ho, Er, Tm, Yb, Lu, and Y) for Environmental and Thermal Barrier Coating Applications, *J. Eur. Ceram. Soc.*, 2016, 36(1), p 189–202.
- E. Bakan, Y.J. Sohn, and R. Vaßen, Metastable to Stable Phase Transformation in Atmospheric Plasma Sprayed Yb-Silicate Coating During Post-Heat Treatment, Scripta Mater., 2023, 225, p. 115169.
- E. Garcia et al., Crystallization Behavior of Air-Plasma-Sprayed Ytterbium-Silicate-Based Environmental Barrier Coatings, J. Eur. Ceram. Soc., 2021, 41(6), p 3696–3705.
- B.T. Richards and H.N.G. Wadley, Plasma Spray Deposition of Tri-Layer Environmental Barrier Coatings, *J. Eur. Ceram. Soc.*, 2014, 34(12), p 3069–3083.
- E. Bakan and R. Vaßen, Crack Healing Mechanisms in Atmospheric Plasma Sprayed Yb-Silicate Coatings During Post-Process Heat Treatment, *J. Eur. Ceram. Soc.*, 2023, 43(8), p 3684–3693.
- S. Kuroda and T.W. Clyne, The Quenching Stress in Thermally Sprayed Coatings, *Thin Solid Films*, 1991, 200(1), p 49–66.
- 22. Matejicek, J., S. Sampath, and H. Herman. Processing effects on splat formation, microstructure and quenching stress in plasma sprayed coatings. in ASM International, Thermal Spray: Meeting the Challenges of the 21 st Century. 1998.
- S.V. Shinde and S. Sampath, Interplay Between Cracking and Delamination in Incrementally Deposited Plasma Sprayed Coatings, *Acta Mater.*, 2021, 215, p 117074.



- M.D. Thouless, E. Olsson, and A. Gupta, Cracking of Brittle Films on Elastic Substrates, *Acta Metall. Mater.*, 1992, 40(6), p 1287–1292.
- J.L. Beuth, Cracking of Thin Bonded Films in Residual Tension, Int. J. Solids Struct., 1992, 29(13), p 1657–1675.
- J. Ilavsky et al., Influence of Spray Angle on the Pore and Crack Microstructure of Plasma-Sprayed Deposits, *J. Am. Ceram. Soc.*, 1997, 80(3), p 733–742.
- A. Kulkarni et al., Processing Effects on Porosity-Property Correlations in Plasma Sprayed Yttria-Stabilized Zirconia Coatings, Mater. Sci. Eng. A, 2003, 359(1), p 100–111.
- S.-H. Leigh and C. Berndt Christopher, Quantitative Evaluation of Void Distributions Within a Plasma-Sprayed Ceramic, *J. Am. Ceram. Soc.*, 2004, 82(1), p 17–21.
- E. Bakan et al., Effect of Processing on High-Velocity Water Vapor Recession Behavior of Yb-Silicate Environmental Barrier Coatings, J. Eur. Ceram. Soc., 2019, 39(4), p 1507–1513.
- R. Vaßen et al., Correlation of Process Conditions, Porosity Levels and Crystallinity in Atmospherically Plasma Sprayed Yb₂Si₂O₇ Environmental Barrier Coatings, *J. Compos. Sci.*, 2021, 5(8), p 198.
- H. Wang et al., Microstructure and Phase Composition Evolution of Dual-Phase Ytterbium Silicate Coatings Plasma Sprayed From Stoichiometric Yb₂Si₂O₇ Feedstock Powder, Surf. Coat. Technol., 2022, 437, p 128373.
- A. Lynam et al., Atmospheric Plasma Spraying of Ytterbium Disilicate for Abradable and Environmental Barrier Coatings: A Story of Processing-Microstructure Relationships, *Ceram. Int.*, 2023, 49(13), p 22232–22243.
- B. Li et al., Influence of Spraying Power on Microstructure, Phase Composition and Nanomechanical Properties of Plasma-Sprayed

- Nanostructured Yb-Silicate Environmental Barrier Coatings, *Surf. Coat. Technol.*, 2024, **478**, p 130450.
- E. Bakan et al., Plasma Sprayed Duplex Ytterbium Disilicate/ Monosilicate EBCs and the Transformation from Ytterbia to Ytterbium Monosilicate During Burner Rig Testing, Corros. Sci., 2024, 235, p 112174.
- 35. P. Gougeon and C. Moreau, In-Flight Particle Surface Temperature Measurement: Influence of the Plasma Light Scattered by the Particles, *J. Therm. Spray Technol.*, 1993, **2**(3), p 229–233.
- V. Srinivasan et al., Particle Injection in Direct Current Air Plasma Spray: Salient Observations and Optimization Strategies, Plasma Chem. Plasma Process., 2007, 27(5), p 609–623.
- S. Sampath and X. Jiang, Splat Formation and Microstructure Development During Plasma Spraying: Deposition Temperature Effects, *Mater. Sci. Eng. A*, 2001, 304–306, p 144–150.
- P. Fauchais et al., Knowledge Concerning Splat Formation: An Invited Review, J. Therm. Spray Technol., 2004, 13(3), p. 337–360.
- T.W. Clyne and S.C. Gill, Residual Stresses in Thermal Spray Coatings and Their Effect on Interfacial Adhesion: A Review of Recent Work, J. Therm. Spray Technol., 1996, 5(4), p 401.
- E.J. Gildersleeve and S. Sampath, Process-Geometry Interplay in the Deposition and Microstructural Evolution of 7YSZ Thermal Barrier Coatings by Air Plasma Spray, *J. Therm. Spray Technol.*, 2020, 29(4), p 560–573.
- 41. E. Pfender, Heat and Momentum Transfer to Particles in Thermal Plasma Flows, *Pure Appl. Chem.*, 1985, **57**(9), p 1179–1195.

Publisher's Note Springer Nature remains neutral with regard to jurisdictional claims in published maps and institutional affiliations.

